ELEG404/604: Imaging & Deep Learning

Gonzalo R. Arce

Department of Electrical and Computer Engineering
University of Delaware

Chapter VIII

X-Ray discovery

In 1895 Wilhelm Rontgen discovered the X-rays, while working with a cathode ray tube in his laboratory. One of his first experiments was a film of his wife's hand.

Shoe Fitting X-Ray Device

Shoe stores in the 1920s until the 1950s installed X-ray fluoroscope machines as a promotion device.

Oak Ridge Associated Universities
Shoe-Fitting Fluoroscope (ca. 1930-1940)

X-Ray Spectrum

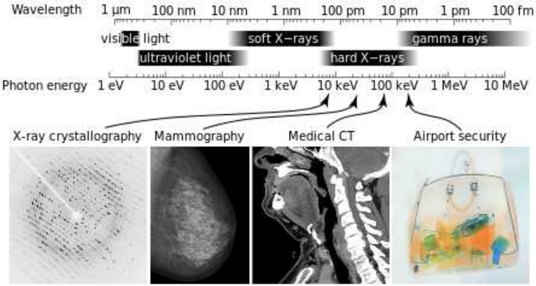

$$E = \hbar \cdot f = \hbar \frac{c}{\lambda}.$$

1 eV is the kinetic energy gained by an electron that is accelerated across a one volt potential.

- **Wavelength**: 0.01 - 10 nm.
- **Frequency**: 30 petahertz ($3x10^{16}$) to 30 exahertz ($3x10^{19}$).
- **Soft X-Rays**: 0.12 to 30 keV.
- **Hard X-Rays**: 30 to 120 keV.

Ionization and Excitation

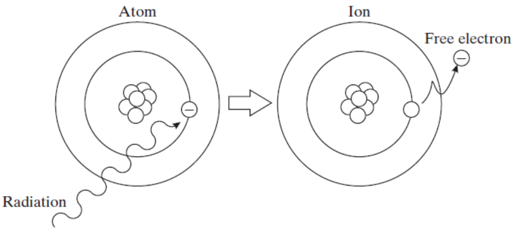

Bound energy < Unbound energy + Electron energy

- **Ionization**: Ejection of an electron from an atom, creating a free electron and an ion. The electron is ejected from the atom if the energy transferred by radiation to it, is equal or greater than the electron's binding energy.
- **Excitation**: Raising of an electron to a higher energy state e.g., an outer orbit.

Ionizing Radiation

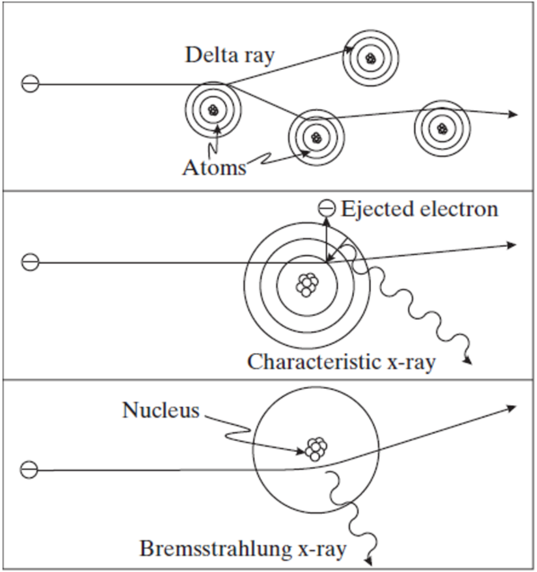

Collisional Transfer
Incident electron collides with other electrons until it loses its kinetic energy.

Characteristic Radiation
Incident electron ejects a K-shell electron generating a characteristic X-ray.

Bremsstrahlung Radiation
Incident electron is “breaked” by a nucleus, generating “breaking” radiation

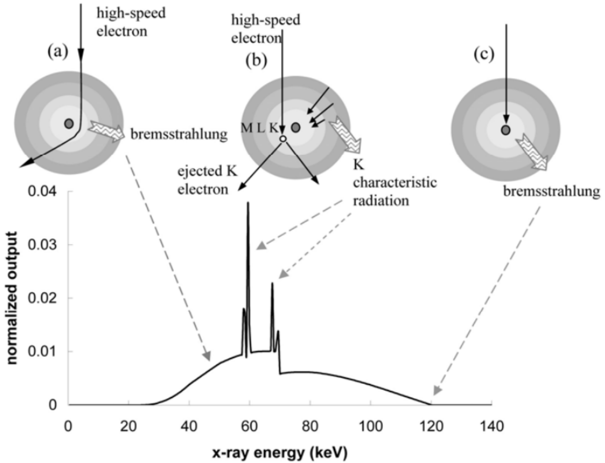

Illustration of electron interaction with a target and its relationship to the x-ray tube energy spectrum. (a) Bremsstrahlung radiation is generated when high-speed electrons are decelerated by the electric field of the target nuclei. (b) Characteristic radiation is produced when a high-speed electron interacts with a target electron and ejects it from its electronic shell. When outer-shell electrons fill in the vacant shell, characteristic x rays are emitted. (c) A high-speed electron hits the nucleus directly, and the entire kinetic energy is converted to x-ray energy. For the x-ray spectrum shown in the figure, the target material is tungsten, and additional filtration is used to remove low-energy x rays.

Spectrum of X-Ray

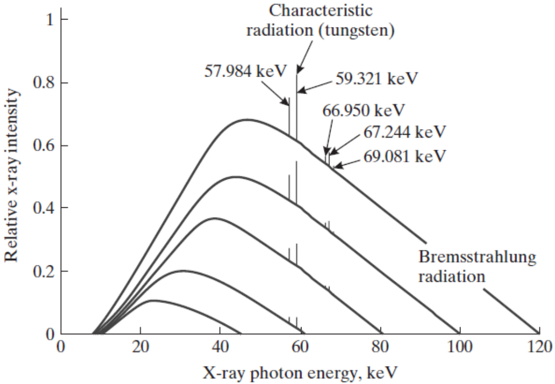

The different curves correspond to different potentials applied to the tube: 45kV, 61kV, 80kV, 100kV and 120 kV. The particular spectral lines correspond to characteristic radiation of Tungsten.

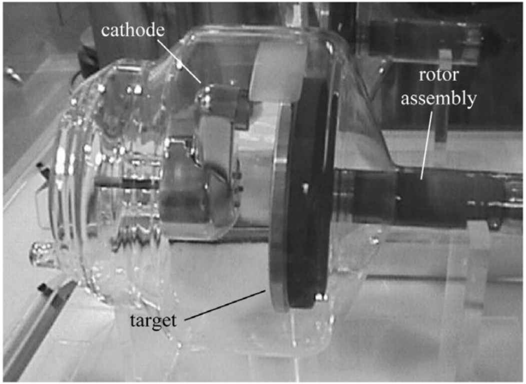

Photograph of an early vintage glass envelope x-ray tube.

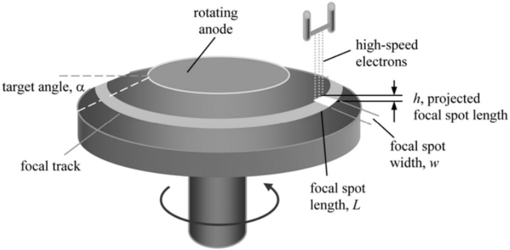

Illustration of a target assembly. The target rotates at a very high speed so that the heat generated by the electron bombardment is distributed over a large area (light gray band on the target). In addition, the target surface is at a shallow angle (α = 7 deg) with respect to the CT scan plane to increase the exposure area while maintaining a small projected focal spot length.

X-Ray interaction with matter

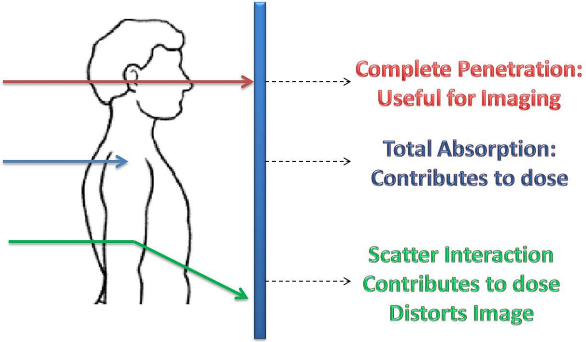

The main mechanisms by which Electromagnetic ionizing radiation interacts with matter are:

- Photoelectric effect
- Compton Scattering
- Pair Production

Compton Scattering

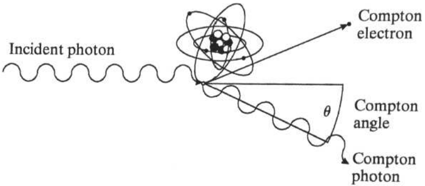

- Photon collides with outer-shell electron, producing a new energetic electron called Compton electron.
- The incident photon, the Compton photon, changes its direction and losses energy as a result of the interaction.
- Undesirable for diagnostic radiography, and represents a source of radiation for the personnel conducting the diagnosis.
- It is as likely to occur with soft tissue as bone.

X-Ray Attenuation

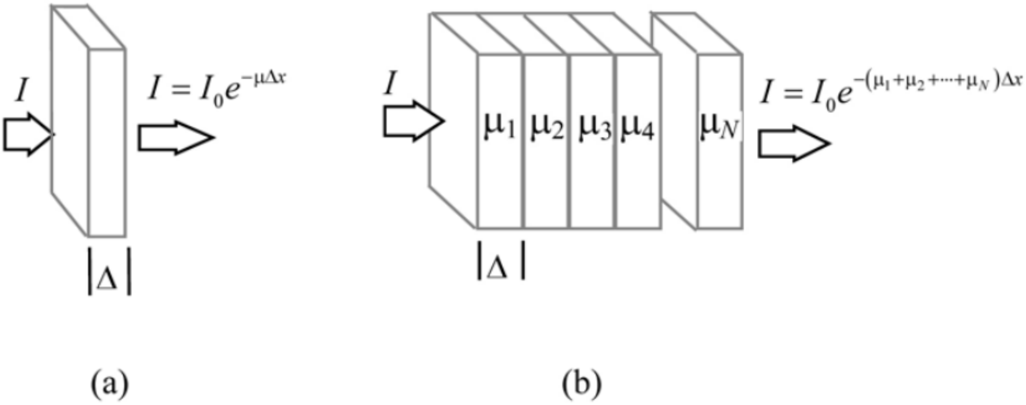

Illustration of material attenuation for a monochromatic x-ray beam. (a) Attenuation of monoenergetic x rays by a uniform object follows the Beer–Lambert law. (b) Any nonuniform object can be subdivided into multiple elements. Within each element, a uniform attenuation coefficient can be assumed. The Beer–Lambert law can then be applied in a cascade fashion.

Linear attenuation coefficient

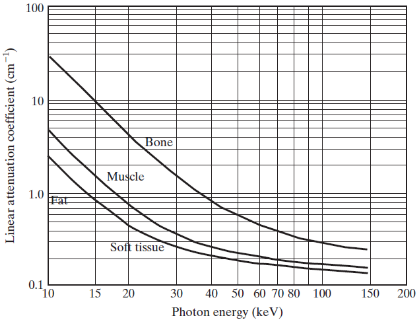

When the slab is non uniform, that is the linear attenuation coefficient varies along the slab, supposing the mono energetic case:

$$I(x) = I_0 e^{-\int_0^x \mu(x')\, dx'}$$

Where $I(x)$ is the x-ray intensity at position x.

Radiation Dose in X-Ray and CT Exams

Doctors use "effective dose" when they talk about the risk of radiation to the entire body. Risk refers to possible side effects, such as the chance of developing a cancer later in life. Effective dose takes into account how sensitive different tissues are to radiation

	Procedure	Approximate effective radiation dose	Comparable to natural background radiation for:
ABDOMINAL REGION 	Computed Tomography (CT)–Abdomen and Pelvis	10 mSv	3 years
	Computed Tomography (CT)–Abdomen and Pelvis, repeated with and without contrast material	20 mSv	7 years
	Computed Tomography (CT)–Colonography	6 mSv	2 years
	Intravenous Pyelogram (IVP)	3 mSv	1 year
	Barium Enema (Lower GI X-ray)	8 mSv	3 years
	Upper GI Study with Barium	6 mSv	2 years

Radiation Dose in X-Ray and CT Exams

BONE

Procedure	Approximate effective radiation dose	Comparable to natural background radiation for:
Spine X-ray	1.5 mSv	6 months
Extremity (hand, foot, etc.) X-ray	0.001 mSv	3 hours

CENTRAL NERVOUS SYSTEM

Procedure	Approximate effective radiation dose	Comparable to natural background radiation for:
Computed Tomography (CT)–Head	2 mSv	8 months
Computed Tomography (CT)–Head, repeated with and without contrast material	4 mSv	16 months
Computed Tomography (CT)–Spine	6 mSv	2 years

Radiation Dose in X-Ray and CT Exams

	Procedure	Approximate effective radiation dose	Comparable to natural background radiation for:
CHEST 			
	Computed Tomography (CT)–Chest	7 mSv	2 years
	Computed Tomography (CT)–Lung Cancer Screening	1.5 mSv	6 months
	Chest X-ray	0.1 mSv	10 days
DENTAL 	**Procedure**	**Approximate effective radiation dose**	**Comparable to natural background radiation for:**
	Dental X-ray	0.005 mSv	1 day

Biological Effects

- The main risk from ionizing radiation at the doses involved in medical imaging is cancer production.
- Injury to living tissue from the transfer of energy to atoms and molecules of the body.
- Can cause acute effects such as: skin reddening, hair loss and radiation burns.
- The general public should not be exposed to more than 100mrem/year.

X-ray Tubes

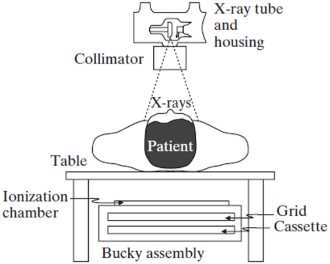

Radiographic system

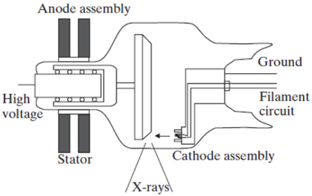

X-ray Tube Diagram

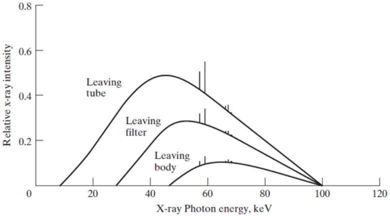

X-ray Spectra

Restriction Beam and Compensation Filters

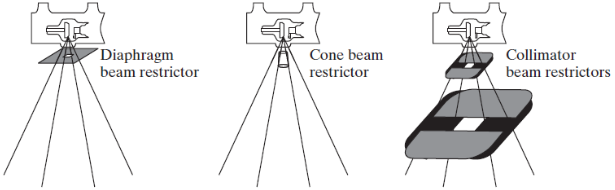

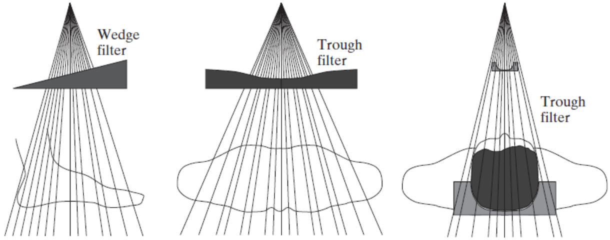

Imaging Equations

Monochromatic X-ray Source:

$$I(x,y) = I_0 e^{-\int_0^{r(x,y)} \mu(s;x,y)\,\mathrm{d}s}$$

Polychromatic X-ray Source:

$$I(x,y) = \int_0^{E_{max}} \left\{ S_0(E')E' e^{-\int_0^{r(x,y)} \mu(s;E',x,y)\,ds}, dE' \right\} \tag{1}$$

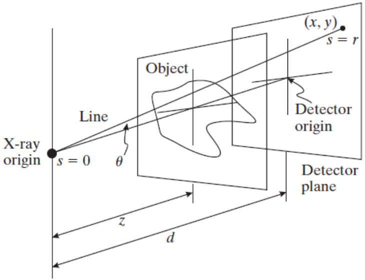

Reconstruction History

Hounsfield's experimental CT:

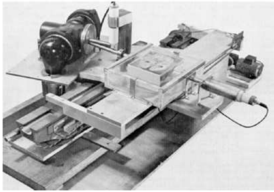

- Reconstruction methods based on Radon's work
  - 1917-classic image reconstruction from projections paper
- 1972 - Hounsfield develops the first commercial x-ray CT scanner

- Hounsfield and Cormack receive the 1979 Nobel Prize for their CT contributions
- Classical reconstruction is based on the Radon transform
  - Method known as backprojection
- Alternative approaches
  - Fourier Transform and iterative series-expansion methods
  - Statistical estimation methods
  - Wavelet and other multiresolution methods
  - Sub-Nyquist sampling: Compressed sensing and Partial Fourier Theories

1^{st} Generation CT: Parallel Projections

Hounsfield's Experimental CT

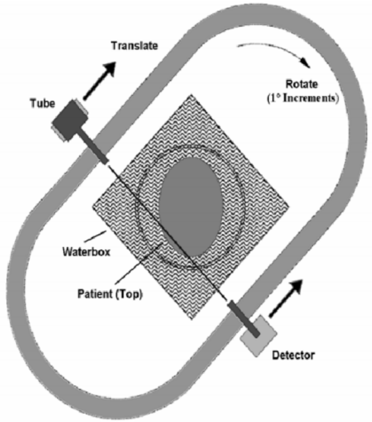

- 1 Beam and 1 Detector
- 160 samples/traverse: 5min
- 1º increments over 180º
- 28,800 samples
- Solved simultaneous equations (Fortran): 2.5h
- 160^2 image matrix but reduced to 80^2 for practical clinical use

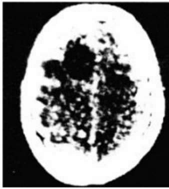

Example

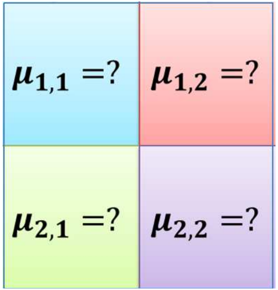

Suppose an object that has 4 materials arranged in the boxes shown above. How can we find the linear attenuation coefficients?

Image Reconstruction

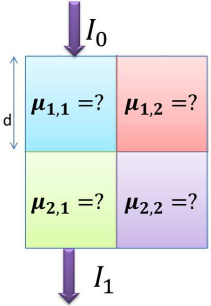

$$I_1 = I_0 e^{-(\mu_{1,1}+\mu_{2,1})d}$$

$$\ln\frac{I_1}{I_0} = -(\mu_{1,1} + \mu_{1,2})d$$

$$(\mu_{1,1} + \mu_{1,2}) = -\frac{1}{d}\ln\frac{I_1}{I_0}$$

Suppose an x-ray of intensity I_0 is passing through the first column of the object, and that I_1 is the intensity measured at the other side.

Image Reconstruction

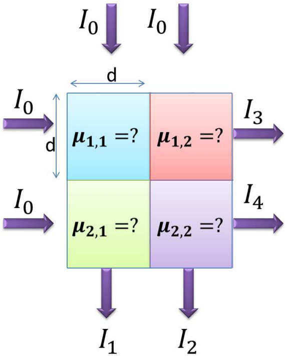

$$(\mu_{1,1} + \mu_{2,1}) = -\frac{1}{d}\ln\frac{I_1}{I_0}$$
$$(\mu_{1,2} + \mu_{2,2}) = -\frac{1}{d}\ln\frac{I_2}{I_0}$$
$$(\mu_{1,1} + \mu_{1,2}) = -\frac{1}{d}\ln\frac{I_3}{I_0}$$
$$(\mu_{2,1} + \mu_{2,2}) = -\frac{1}{d}\ln\frac{I_4}{I_0}$$

If we repeat the same process for each of the rows and the columns, we obtain the equations necessary to obtain the values of the coefficients.However for bigger systems, the number of equations is not practical for implementation.

Radon Transform

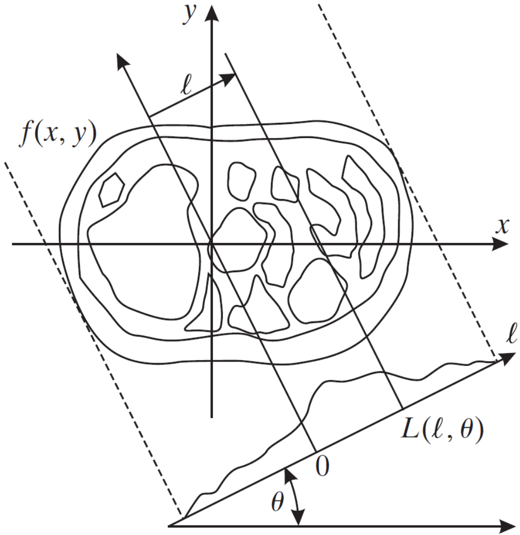

- $f(x,y)$ describes our object
- How to describe $f(x,y)$ in terms of its projections onto a line c
- Let ℓ be the distance along the line $L(\ell,\theta)$ starting from the origin.

Radon Transform

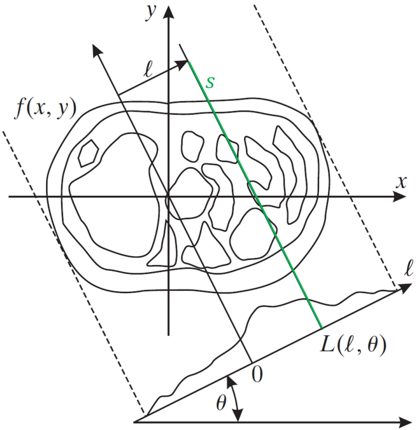

- For a fixed projection angle θ, and a particular linear shift of the X-ray beam, a projection integral is given by:

$$g(\ell,\theta)=\int_{-\infty}^{\infty} f(x(s),y(s))ds$$

- Example: If $\theta=0$

$$g(\ell,\theta=0)=\int_{-\infty}^{\infty} f(\ell,y)dy$$

- Example: If $\theta=90$

$$g(\ell,\theta=90)=\int_{-\infty}^{\infty} f(x,\ell)dx$$

Radon Transform $\forall\theta$

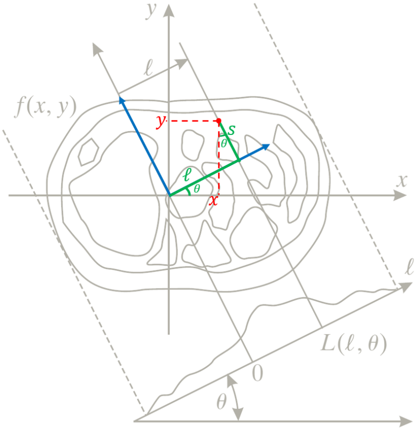

Option 1

Rotate the coordinate system so that ℓ and the projection direction (axis of integration) are horizontal and vertical

$$\begin{aligned} x(s) &= \ell\cos\theta - s\sin\theta \\ y(s) &= \ell\sin\theta + s\cos\theta \end{aligned}$$

$$g(\ell,\theta) = \int_{-\infty}^{\infty} f(x(s), y(s))\,ds$$

Radon Transform $\forall\theta$

Option 2

Instead of rotating the object and integrating, integrate the object only along the line $L(\ell,\theta)$

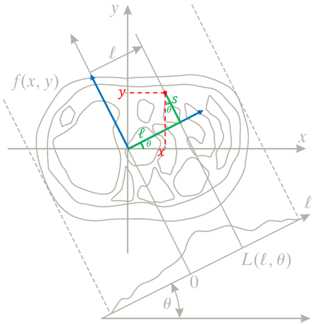

$$g(\ell,\theta) = \int_{-\infty}^{\infty}\int_{-\infty}^{\infty} f(x,y)\delta(x\cos\theta + y\sin\theta - \ell)dxdy$$

- The sifting property causes the integrand to be zero everywhere except on $L(\ell,\theta)$

How does the Radon Transform apply to X-rays

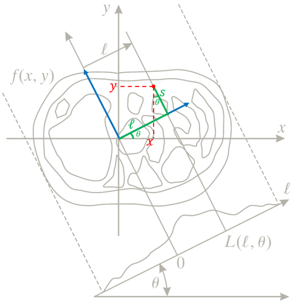

$$x(s) = \ell\cos\theta - s\sin\theta$$
$$y(s) = \ell\sin\theta + s\cos\theta$$

$$g(\ell,\theta) = \int_{-\infty}^{\infty} f(x(s),y(s))ds$$

Recall that $I_d = I_0 \exp\left(-\int_0^d \mu(x(s),y(s))ds\right)$ is the received X-ray intensity of a beam projected through an object along the line s. Taking logarithms at both sides:

$$-\ln\left(\frac{I_d}{I_0}\right) = \int_0^d \mu(x(s),y(s))ds$$

Then the Radon transforms describes the X-ray projections for $g(\ell,\theta) = -\ln\left(\frac{I_d}{I_0}\right)$ and $f(x,y) = \mu(x,y)$.

How does the Radon Transform apply to X-rays

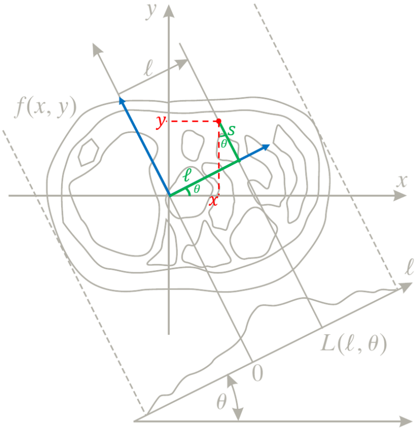

Radon Transform

In CT we measure $g(\ell,\theta) = -\ln\left(\frac{I_d}{I_0}\right)$ and need to find $f(x,y) = \mu(x,y)$ using

$$
\begin{aligned}
g(\ell,\theta) &= \int_{-\infty}^{\infty} f(x(s),y(s))ds \\
x(s) &= \ell\cos\theta - s\sin\theta \\
y(s) &= \ell\sin\theta + s\cos\theta
\end{aligned}
$$

Sinogram

A sinogram is an image of $g(\ell, \theta)$

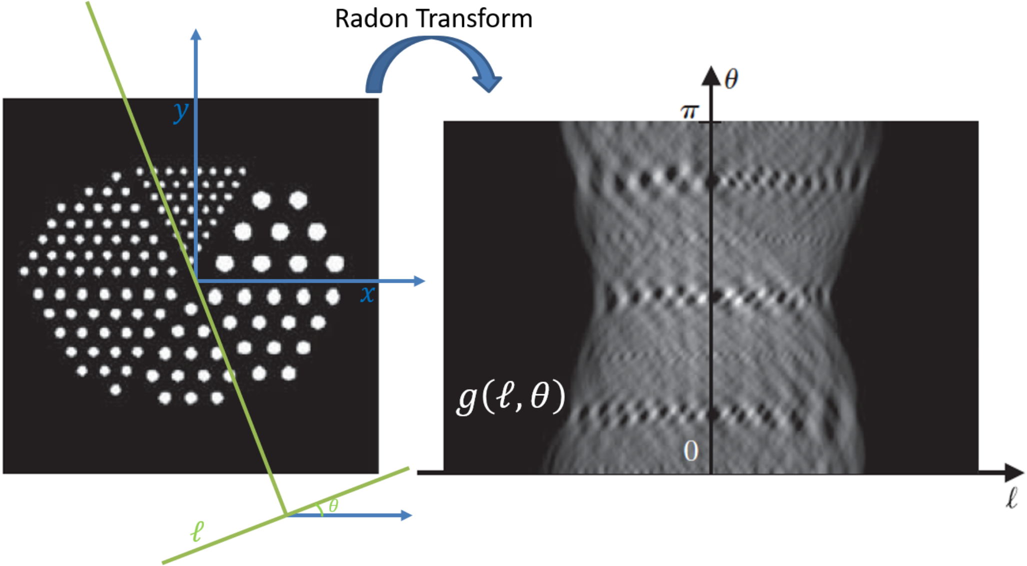

Back Projection Method

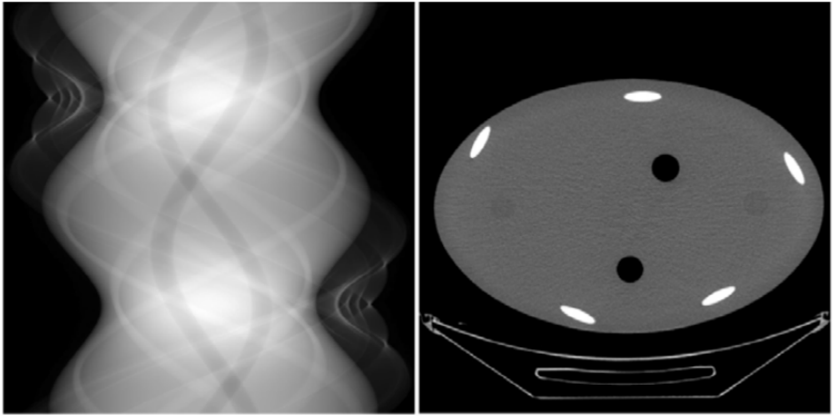

(a) (b)

(a) Sinogram and (b) the object. The sinogram of any complicated object is formed with overlapping sinusoidal curves, since any object can be considered a collection of many small points.

Backprojection Method

Intuition: If $g(\ell, \theta_0)$ takes on a large value at $\ell = \ell_0$, then $f(x,y)$ must be large over the line (or somewhere on the line) $L(\ell_0, \theta_0)$.

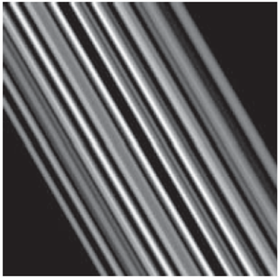

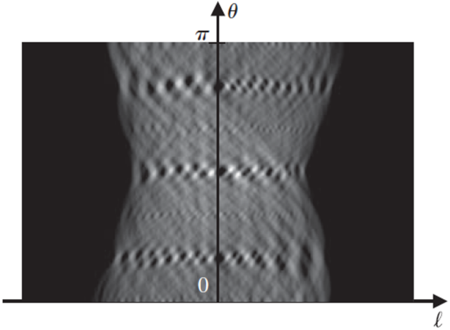

One way to create an image with this property is to assign every point on $L(\ell_0, \theta_0)$ the value $g(\ell_0, \theta_0)$, i.e. $b_\theta = g(x\cos\theta + y\sin\theta, \theta)$.

Back Projection Example

With the example of the 4 boxes given before, we back project the results obtained. As it can be seen, the right answer is not obtained, however the order of the numbers is the same:

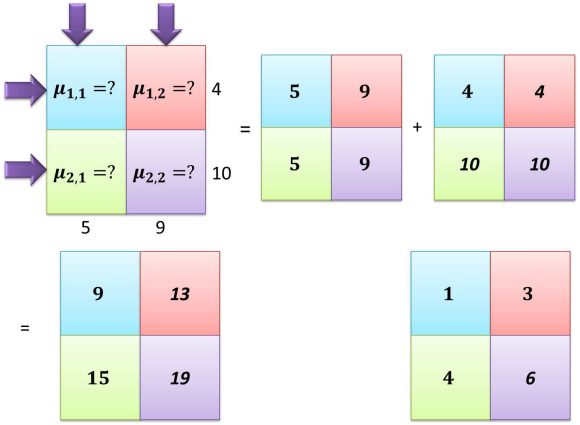

Problems with Backprojection Method

- Bright spots tend to reinforce, which results in a blurry image.
- Problem:

$$f_b(x,y) = \int_0^{\pi} b_\theta(x,y)d\theta \neq f(x,y)$$

- Resulting Image (Laminogram):

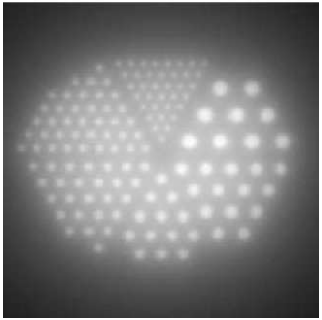

Back Projection Method

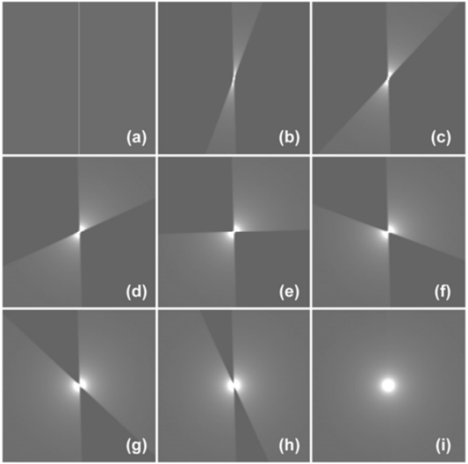

Backprojection process of a single point. (a) Backprojected image of a single projection. (b)–(i) Backprojection of views covering: (b) 0 to 22.5 deg; (c) 0 to 45 deg; (d) 0 to 67.5 deg; (e) 0 to 90 deg; (f) 0 to 112.5 deg; (g) 0 to 135 deg; (h) 0 to 157.5 deg; and (i) 0 to 180 deg.

Projection-Slice Theorem

Take the 1D Fourier transform of a projection $g(\ell, \theta)$

$$G(\rho, \theta) = \mathcal{F}_{1D}\{g(\ell, \theta)\} = \int_{-\infty}^{\infty} g(\ell, \theta) e^{-j2\pi\rho\ell} d\ell$$

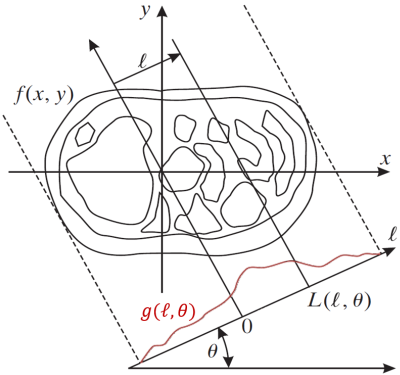

Projection Slice Theorem

From the 1D Fourier Transform of a projection $g(\ell,\theta)$

$$G(\rho,\theta) = \mathcal{F}_{1D}\left\{g(\ell,\theta)\right\} = \int_{-\infty}^{\infty} g(\ell,\theta)e^{-j2\pi\rho\ell}d\ell$$

Next we substitute the Radon transform for $g(\ell,\theta)$

$$\begin{aligned} g(\ell,\theta) &= \int_{-\infty}^{\infty}\int_{-\infty}^{\infty} f(x,y)\delta(x\cos\theta + y\sin\theta - \ell)dxdy \\ G(\rho,\theta) &= \int_{-\infty}^{\infty}\int_{-\infty}^{\infty}\int_{-\infty}^{\infty} f(x,y)\delta(x\cos\theta + y\sin\theta - \ell)e^{-j2\pi\rho\ell}dxdyd\ell \end{aligned}$$

Rearranging

$$G(\rho,\theta) = \int_{-\infty}^{\infty}\int_{-\infty}^{\infty} f(x,y)\left\{\int_{-\infty}^{\infty}\delta(x\cos\theta + y\sin\theta - \ell)e^{-j2\pi\rho\ell}d\ell\right\}dxdy$$

Projection-Slice Theorem

What does this look like?

$$
\begin{aligned}
G(\rho,\theta) &= \int_{-\infty}^{\infty}\int_{-\infty}^{\infty} f(x,y)\left\{e^{-j2\pi\rho[x\cos\theta+y\sin\theta]}\right\}dxdy \\
G(\rho,\theta) &= \int_{-\infty}^{\infty}\int_{-\infty}^{\infty} f(x,y)\left\{e^{-j2\pi[x\rho\cos\theta+y\rho\sin\theta]}\right\}dxdy
\end{aligned}
$$

It is reminiscent of the 2D Fourier transform of $f(x,y)$, defined as

$$F(u,v) = \int_{-\infty}^{\infty}\int_{-\infty}^{\infty} f(x,y)e^{-j2\pi(xu+yv)}dxdy$$

Let $u = \rho\cos\theta$ and $v = \rho\sin\theta$, then

$$G(\rho,\theta) = F(\rho\cos\theta, \rho\sin\theta)$$

Projection-Slice Theorem

The 1-D Fourier transform of a projection is a *slice* of the 2D Fourier transform of the object

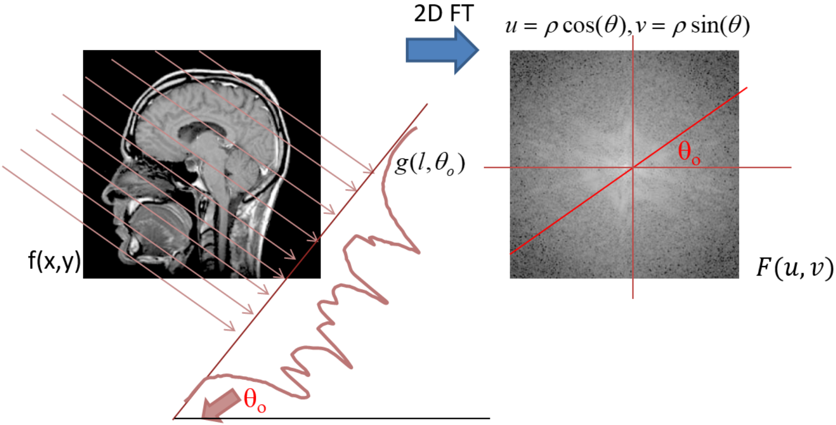

Fourier Reconstruction Method

Take projections at all angles θ. Take the 1D FT to build $F(u,v)$ one slice at a time. Take the Inverse 2D-FT of the result.

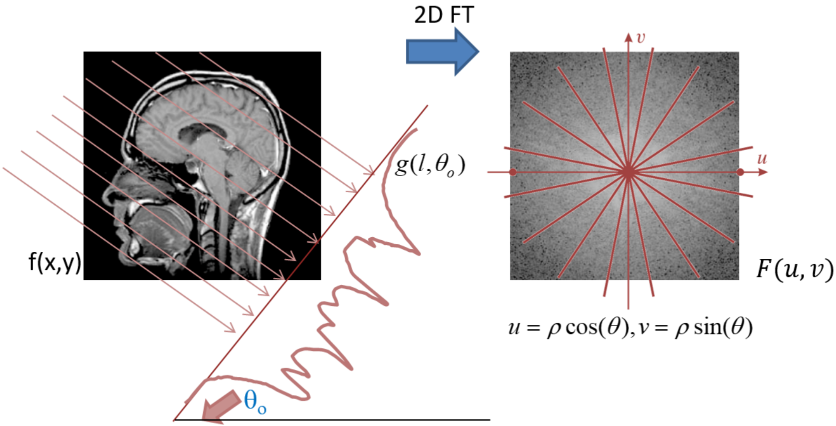

Fourier Reconstruction Method

- The projection slice theorem leads to the following reconstruction method:
  - Take 1D Fourier Transform of each projection to obtain $G(\rho, \theta)$ for all θ.
  - Convert $G(\rho, \theta)$ to Cartesian grid $F(u, v)$.
  - Take inverse 2D Fourier Transform to obtain f(x,y).
- It is not used because it is difficult to interpolate polar data into a Cartesian grid, and the inverse 2D Fourier Transform is time consuming

Filtered Back Projection

Consider the inverse Fourier Transform in 2D: In polar coordinates , $u = \rho\cos\theta$ and $v = \rho\sin\theta$, the inverse Fourier transform can be written as

$$f(x,y) = \int_0^{2\pi}\int_0^{\infty} F(\rho\cos\theta, \rho\sin\theta)e^{j2\pi\rho[x\cos\theta + y\sin\theta]}\rho d\rho d\theta$$

Using the projection-slice theorem $G(\rho,\theta) = F(\rho\cos\theta, \rho\sin\theta)$, we have

$$f(x,y) = \int_0^{2\pi}\int_0^{\infty} G(\rho,\theta)e^{j2\pi\rho[x\cos\theta + y\sin\theta]}\rho d\rho d\theta$$

Since $g(\ell,\theta) = g(-\ell,\theta+\pi)$ it follows that

$$f(x,y) = \int_0^{\pi}\int_{-\infty}^{\infty} |\rho| G(\rho,\theta) e^{j2\pi\rho[x\cos\theta + y\sin\theta]} d\rho d\theta.$$

Furthermore, from the integration over ρ, the term $x\cos\theta + y\sin\theta$ is a constant, say ℓ. Hence,

$$f(x,y) = \int_0^{\pi}\left[\int_{-\infty}^{\infty} |\rho| G(\rho,\theta) e^{j2\pi\rho\ell} d\rho\right] d\theta$$

- Filter Response.
  - $c(\rho) = |\rho|$.
  - High pass filter.
- $G(\rho,\theta)$ is more densely sampled when ρ is small.
- The ramp filter compensate for the sparser sampling at higher ρ.

Convolution Back Projection

From the filtered back projection algorithm we get

$$f(x,y) = \int_0^\pi \left[\int_{-\infty}^{\infty} |\rho| G(\rho,\theta) e^{j2\pi\rho\ell} d\rho \right] d\theta$$

From the convolution theorem of the FT, we can rewrite $f(x,y)$ as

$$f(x,y) = \int_0^\pi \left[\mathcal{F}_{1D}^{-1}\{|\rho|\} * g(\ell,\theta) \right] d\theta.$$

Defining $c(\ell) = \mathcal{F}_{1D}^{-1}\{|\rho|\}$,

$$\begin{aligned} f(x,y) &= \int_0^\pi [c(\ell) * g(\ell,\theta)]\, d\theta \\ &= \int_0^\pi \int_{-\infty}^{\infty} g(\ell,\theta) c(x\cos\theta + y\sin\theta - \ell) d\ell d\theta \end{aligned}$$

Problem: $c(\ell)$ does not exist, since $|\rho|$ is not integrable.

Convolution Back Projection

Practical Solution: Windowing ρ

Define

$$\tilde{c}(\ell) = \mathcal{F}_{1D}^{-1}\{|\rho| W(\rho)\},$$

where $W(\rho)$ is a windowing function that filters the observed projection in addition to the ramp filter.

$$f(x,y) = \int_0^{\pi} [\tilde{c}(\ell) * g(\ell,\theta)]\, d\theta$$

Common windows

- Hamming window
- Lanczos window (Sinc function)
- Simple rectangular window
- Ram-Lak window
- Kaiser window
- Shepp-Logan window

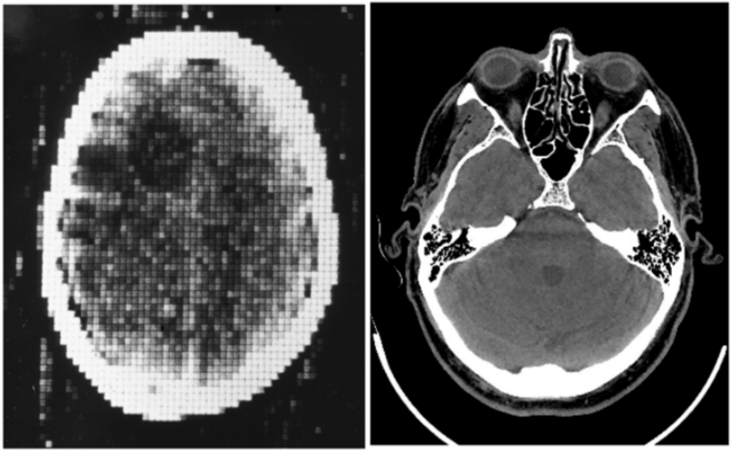

(a) (b)

Comparison of CT head images acquired on (a) one of the first CT scanners and (b) the GE LightSpeed VCT 2005.

2^{nd} Generation

- Incorporated linear array of 30 detectors
- More data acquired to improve image quality
- Shortest scan time was 18 seconds/slice
- Narrow fan beam allows more scattered radiation to be detected

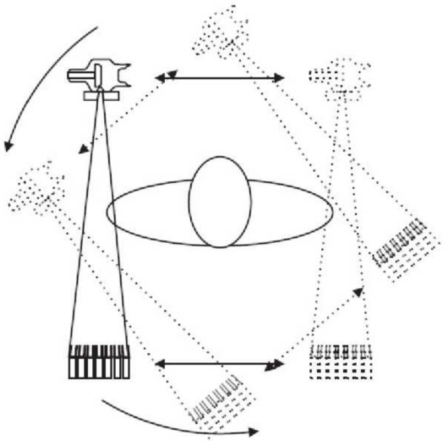

2^{nd} Generation

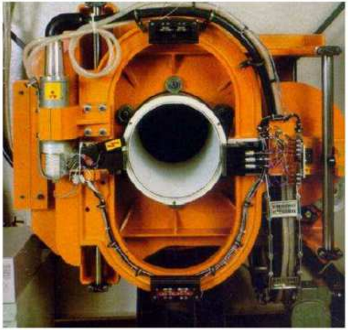

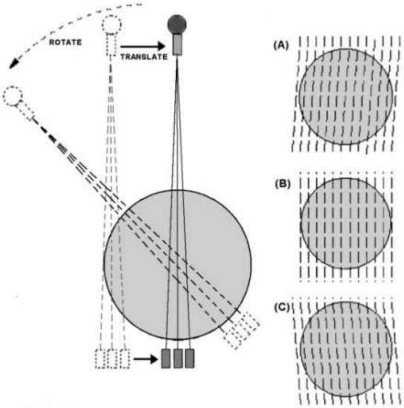

- Multiple detectors
- Still translate-rotate
  - 1 view acquired per detector (~1° apart)
  - angular increment increased by using more detectors

3^{rd} Generation

- Number of detectors increased substantially (more than 800 detectors)
- Angle of fan beam increased to conver entire patient (no need for translational motion)
- Mechanically joined x-ray tube and detector array rotate together
- Newer systems have scan times of $1/2$ second

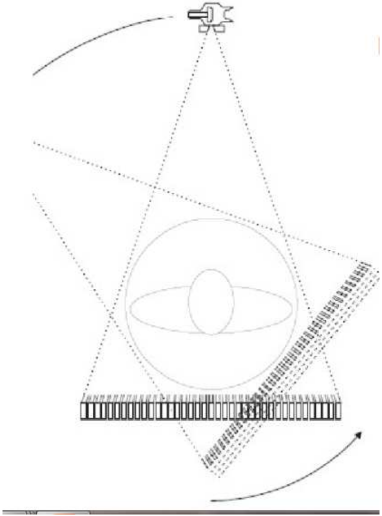

2^{nd} and 3^{rd} Generation Reconstructions

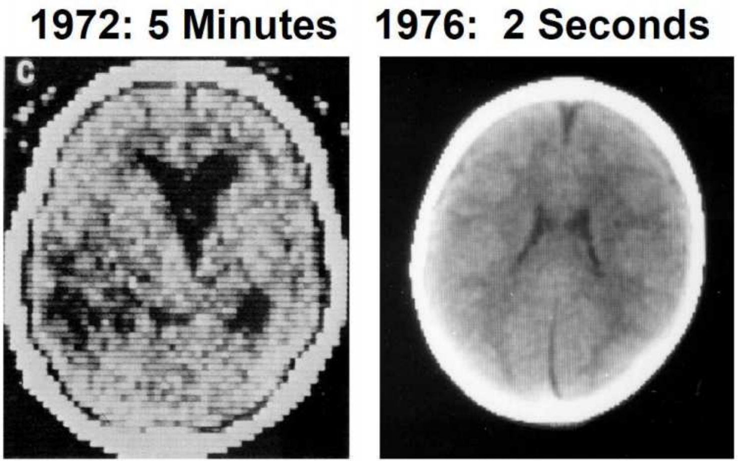

2G

3G

3^{rd} Generation Artifacts

Ring Artifacts

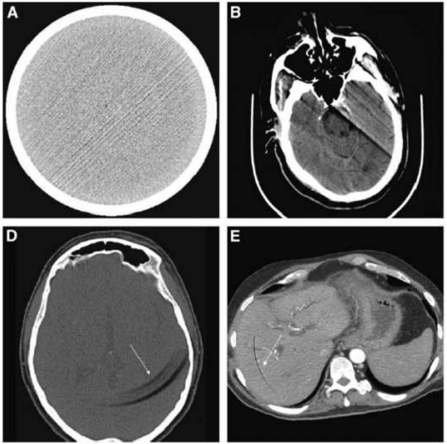

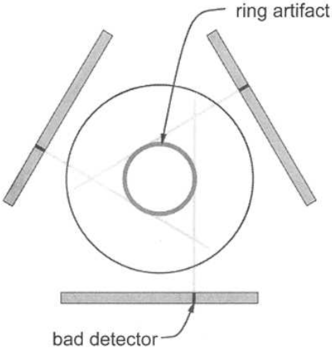

4^{th} Generation

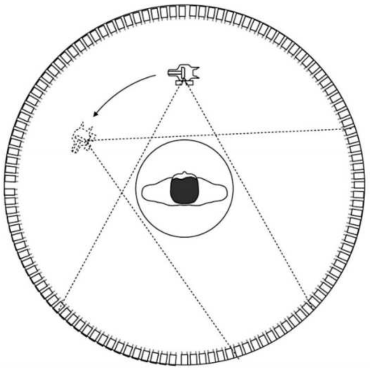

Designed to overcome the problem of artifacts. Stationary ring of about 4800 detectors

Fan Beam Reconstruction

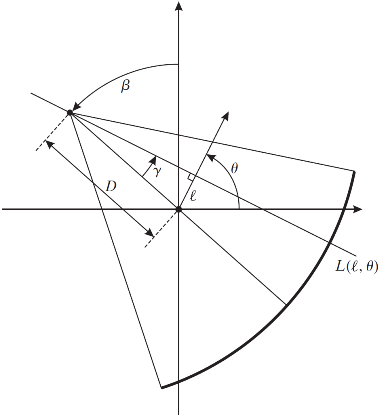

- Fan-beam parameters

$$\begin{aligned}\theta &= \beta+\gamma\\ \ell &= D\sin\gamma,\end{aligned}$$

- D is the distance from source to the origin (isocenter)
- Recall the parallel-ray CBP

$$f(x,y)=\int_0^{\pi}\int_{-\infty}^{\infty} g(\ell,\theta)c(x\cos\theta+y\sin\theta-\ell)d\ell d\theta$$

- Assuming $g(\ell,\theta)=0$ for $|\ell|>T$.

$$f(x,y)=\frac{1}{2}\int_0^{2\pi}\int_{-T}^{T} g(\ell,\theta)c(x\cos\theta+y\sin\theta-\ell)d\ell d\theta$$

Fan Beam Reconstruction

- Let (r, ϕ) be the polar coordinates of a point (x, y). Then $x = r\cos\phi$, $y = r\sin\phi$ and $x\cos\theta + y\sin\theta = r\cos\theta\cos\phi + r\sin\phi\sin\theta = r\cos(\theta-\phi)$. Then:

$$f(r,\phi) = \frac{1}{2}\int_0^{2\pi}\int_{-T}^{T} g(\ell,\theta)c(r\cos(\theta-\phi)-\ell)d\ell d\theta$$

- Using the Jacobian of the transformation: $\theta = \beta+\gamma$ and $\ell = D\sin\gamma$.

$$f(r,\phi) = \frac{1}{2}\int_{-\gamma}^{2\pi-\gamma}\int_{\sin^{-1}\frac{-T}{D}}^{\sin^{-1}\frac{T}{D}} g(D\sin\gamma, \beta+\gamma)c(r\cos(\beta+\gamma-\phi)-D\sin\gamma)D\cos\gamma d\gamma d\beta$$

- The expresion $\sin^{-1}\frac{T}{D}$ represents the largest angle that needs to be considered given an object of radius T, γ_m. Furthermore, functions are periodic in β with period 2π, then:

$$f(r,\phi) = \frac{1}{2}\int_0^{2\pi}\int_{-\gamma_m}^{\gamma_m} p(\gamma,\beta)c(r\cos(\beta+\gamma-\phi)-D\sin\gamma)D\cos\gamma d\gamma d\beta$$

Fan Beam Reconstruction

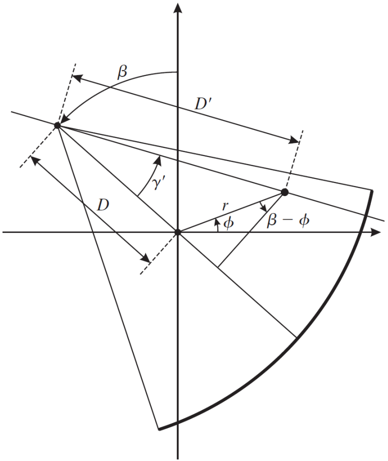

- The argument of $c(\cdot)$ can be written in simpler form using these coordinates

$$r\cos(\beta+\gamma-\phi)-D\sin\gamma = D'\sin(\gamma'-\gamma)$$

- Then, the reconstruction can be rewritten as

$$f(r,\phi)=\frac{1}{2}\int_0^{2\pi}\int_{-\gamma_m}^{\gamma_m} p(\gamma,\beta)c(D'\sin(\gamma'-\gamma))D\cos\gamma d\gamma d\beta$$

- Recall $c(\ell)=\int_{-\infty}^{\infty}|\rho|e^{j2\pi\rho\ell}d\rho$. Then:

$$c(D'\sin(\gamma))=\int_{-\infty}^{\infty}|\rho|e^{j2\pi\rho D'\sin(\gamma)}d\rho$$

Fan-Beam Reconstruction

If we substitute $\rho' = \frac{\rho D' \sin(\gamma)}{\gamma}$, in $c(D' \sin(\gamma)) = \int_{-\infty}^{\infty} |\rho| e^{j2\pi\rho D' \sin(\gamma)} d\rho$. It can be shown that

$$c(D' \sin(\gamma)) = \left(\frac{\gamma}{D' \sin(\gamma)}\right)^2 c(\gamma').$$

Let $c_f = \frac{1}{2} D \left(\frac{\gamma}{\sin(\gamma)}\right)^2 c(\gamma)$, then

$$f(r, \phi) = \int_0^{2\pi} \int_{-\gamma_m}^{\gamma_m} \tilde{p}(\gamma, \beta) c_f(\gamma' - \gamma) d\gamma d\beta,$$

where $\tilde{p}(\gamma, \beta) = \cos(\gamma) p(\gamma, \beta)$

5G: Electron Beam CT (EBCT)

- Developed specifically for cardiac tomographic imaging.
- No conventional x-ray tube; large arc of tungsten encircles patient and lies directly opposite to the detector ring
- Electron beam steered around the patient to strike the annular tungsten target.

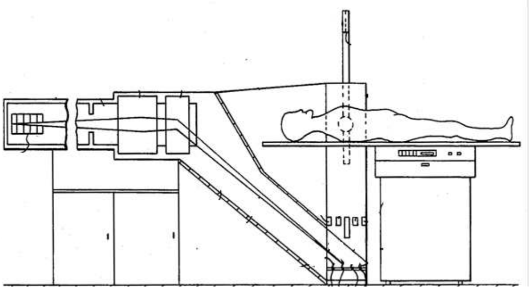

6G and 7G CT

6G: Electron Beam CT (EBCT)

- Helical CT scanners acquire data while the table moves, there is a single detector array.
- Allows the use of less contrast agent.

7G: Multislice

- CT becomes a cone beam
- 40 parallel detector rows
- 32mm detector length
- 16 0.5mm slices for second

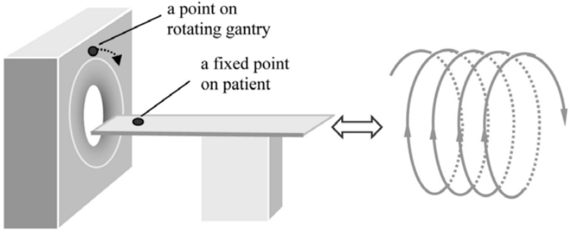

Illustration of helical scan. In a helical scan mode, the traveling path of a point on the rotating gantry viewed by a fixed point on the patient is a helix.

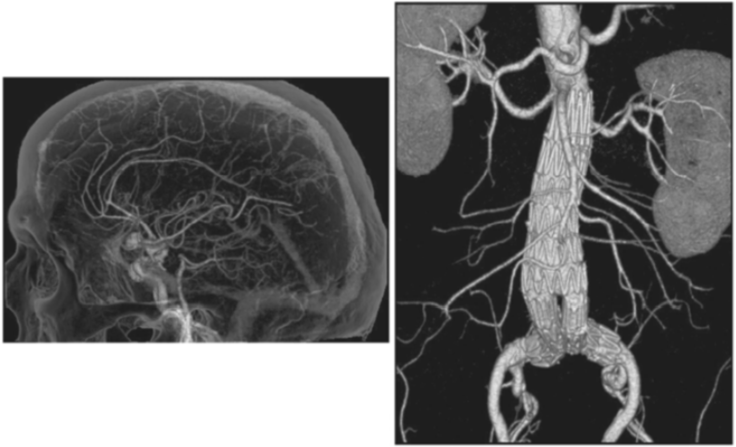

(a) (b)

Volume-rendered images of CTA studies. (a) Neural CT angiogram and (b) abdominal CT angiogram.

(a) (b)

Images of a runoff study. (a) Multiplanar reformed and (b) volume rendered.

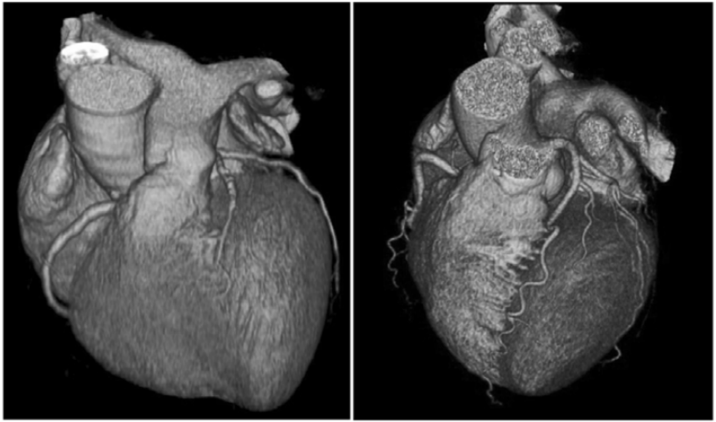

(a) (b)

Examples of 3D volume-rendering cardiac CT images. (a) Data collected on a LightSpeed™ 8-slice scanner. (b) Data collected on a Discovery™ CT750 HD scanner.

Surface-rendered image of a CT scan of an ankle.

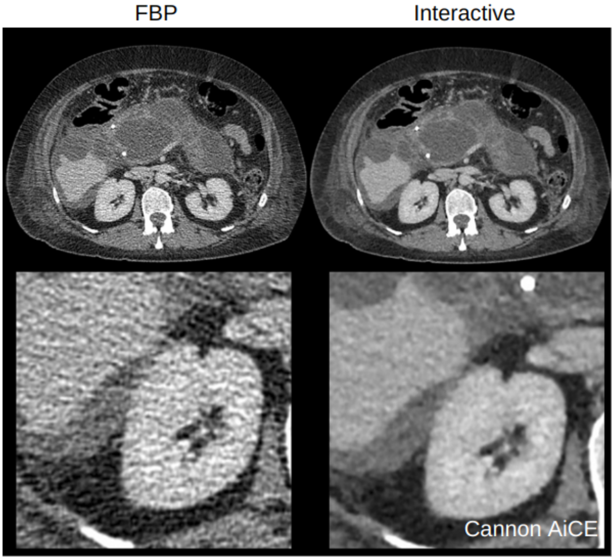

$Noise \propto \frac{1}{\sqrt{Dose}}$ $Noise \propto low\ frequencies$

J. Wang, D. Fleischmann, Radiology 2018:289
T. Szcykutowicz et. Al, Curr. Radiol. Rep 2022:10

Coronal images of a super-low-dose patient CT scan (a) reconstructed with FBP and (b) reconstructed with iterative reconstruction.

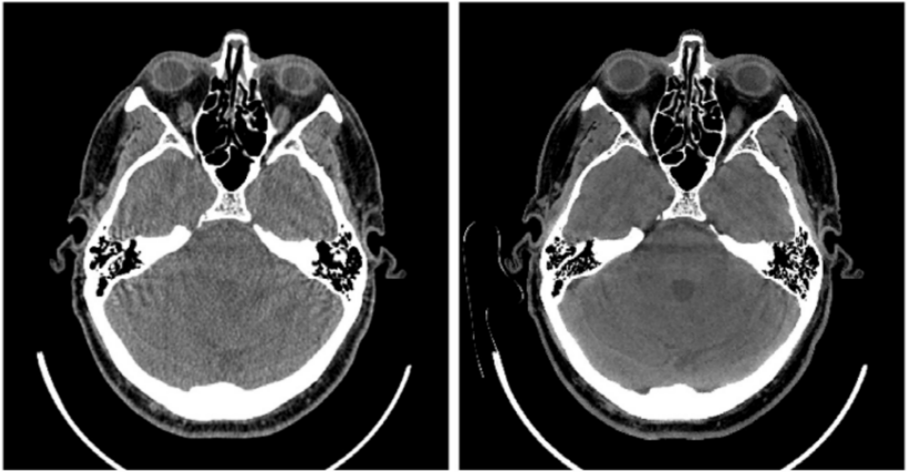

(a) (b)

Axial images of a patient head scan (a) reconstructed with FBP, and (b) reconstructed with iterative reconstruction.

Interactive

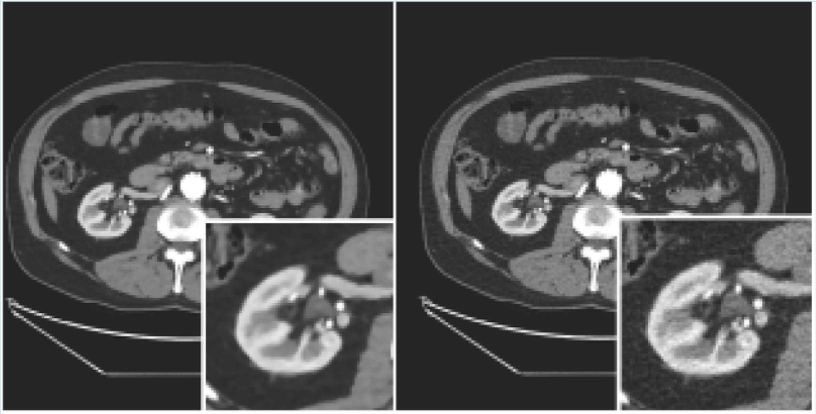

T. Szczykutowicz, The CT Handbook. Medical Physics Publishing; 2020.

Canon AiDRTM, GE ASiRTM, iDose4, Siemens SAFIRE, Siemens IRIS, GE AsiR-V, Canon FIRST, Siemens ADMIRE, Philips IMR, Canon FIRST, GE VeoTM.

IR: Better performance at high-contrast levels

"*Radiologists need be aware, IR reduces spatial resolution in low-contrast*"

Interactive

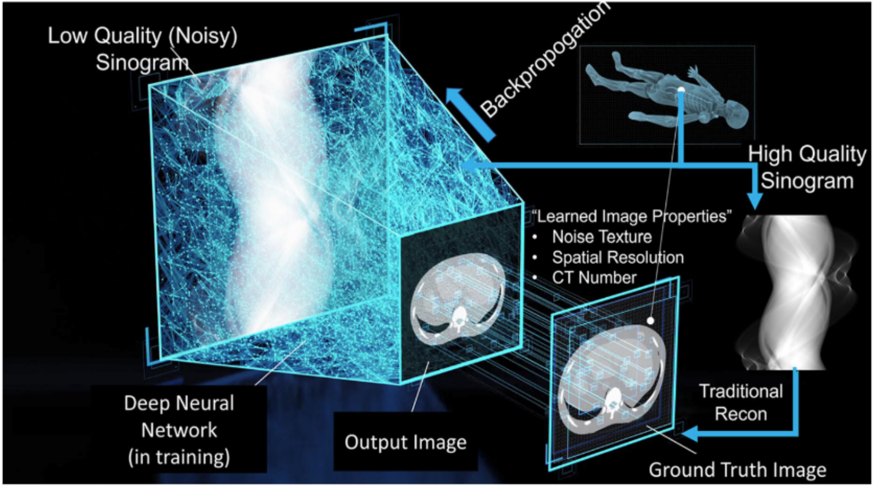

Deep NN training to take noisy CT projection and reconstruct high quality (*denoised*) images

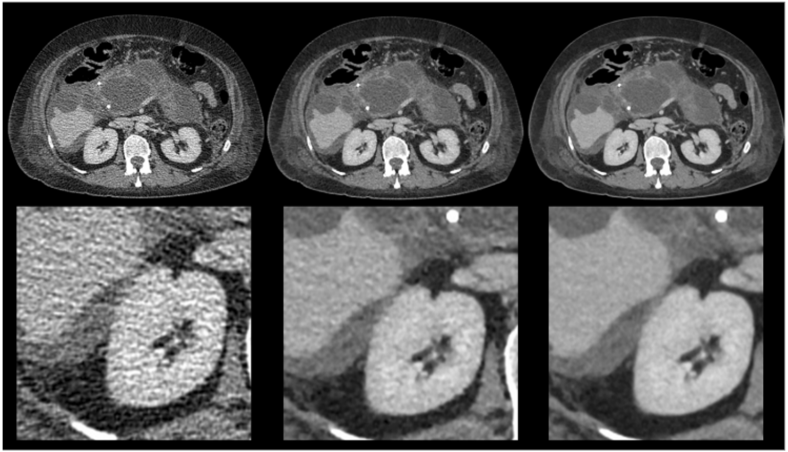

FBP IR DL

Images courtesy of Cannon Medical Systems
T. Szczykutowicz, et. Al, Curr. Radiol. Rep 2022:10.

Deep NN training to take noisy CT projection and reconstruct high quality (*denoised*) images

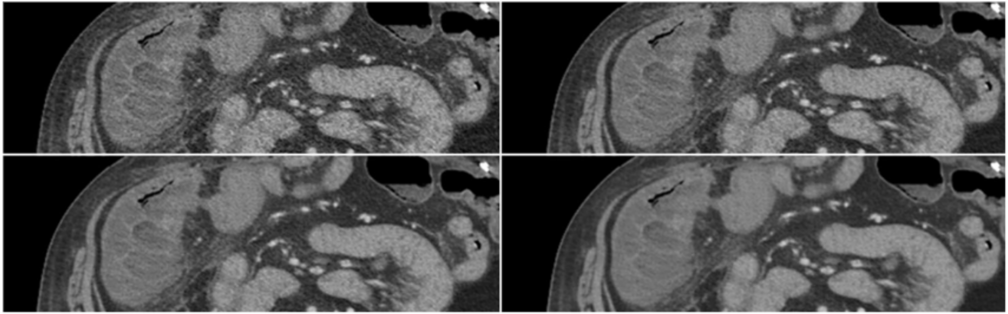

Canon AiCE, GE TrueFidelityTM, Philips Incisive

All radiology readers rated reduced dose (60%-80%) DLR superior to full dose FBP

T. Szczykutowicz, et. Al, Curr. Radiol. Rep 2022:10.